Supercritical Carbon Dioxide-Processed Dispersed Polystyrene−Clay Nanocomposites

Mihai Manitiu, Robert J. Bellair, Steven Horsch, Esin Gulari, and Rangaramanujam M. Kannan*

Department of Chemical Engineering and Materials Science, Wayne State University, 1121 Engineering, 5050 Anthony Wayne Drive, Detroit, Michigan 48202

Received June 13, 2008; Revised Manuscript Received September 3, 2008

ABSTRACT: Achieving clay dispersion and improving clay−polymer interactions are keys to producing superior nanocomposites. A supercritical CO_2 ($scCO_2$) processing method was utilized to prepare high molecular weight polystyrene (PS)/Cloisite 10A nanocomposites with significant dispersion and rheological enhancement. The effects of $scCO_2$ processing, presence of cosolvent, and clay weight fraction on clay dispersion and polymer−clay interactions in nanocomposites were investigated. Rheology, WAXD, and TEM of the nanocomposites indicate that substantial improvements in the rheological properties of $scCO_2$ nanocomposites are the result of increased dispersion and polymer−clay interactions. At low frequencies, the elastic plateau modulus of the $scCO_2$-processing nanocomposites (5 wt % clay loading) is more than 40-fold higher than benchmark solution-blended samples. Our results suggest that the substantial contacting with $scCO_2$, followed by rapid depressurization, produces a combination of disorder and dispersion of this "as-received" clay, and the presence of the cosolvent enables more intimate contact of the high molecular weight PS and clay.

1. Introduction

Polymer−clay nanocomposites have the potential to offer large improvements in barrier properties, tensile strength, thermal stability, and processability. Increased performance is dependent on the extent of platelet dispersion and degree of polymer−clay and clay−clay interactions.[1−3] The small equilibrium spacing of natural clay (∼1 nm) as well as its inherent hydrophilicity makes polymer penetration unfavorable and therefore limits access to the large potential surface area. Due to this limitation, clay is generally modified with an organophilic quaternary ammonium ion, whose purpose is 2-fold: the modifier improves compatibility/miscibility between the polymer and clay, and it increases the equilibrium spacing between the platelets facilitating polymer penetration.[4,5]

Although nanoclays have been successfully intercalated or exfoliated in many polar polymers such as polyamides[6,7] and epoxides,[8,9] dispersing clay in industrially important polymers with low polarity such as polystyrene, polypropylene, and polyethylene has proven to be more challenging.[10−15] The most common strategies for processing nonpolar polymer/clay nanocomposites fall into three categories: (i) mechanical compounding/melt mixing, (ii) in-situ polymerization, and (iii) solution blending.

Mechanical compounding is the preferable method from an industrial point of view because of the short processing times, the absence of solvents, and the compatibility with industrial manufacturing techniques; however, it has had limited success in the absence of compatabilizers.[15−17] In addition, the elevated temperatures needed to reduce processing time and promote chain diffusion into the galleries degrades the organic modifier, causing the tactoids to collapse.[18] Typically, polar compatibilizers and copolymers are utilized to increase the intergallery spacing, weakening the platelet−platelet interaction and increasing the polymer−platelet interaction allowing for better coupling of the shear force to the platelet.[15,19]

In-situ polymerization of monomers between clay layers has been shown to give a wide range of dispersion with varying levels of property enhancements depending on the polymerization scheme used.[20−25] A high level of complexity is involved due to the need for specialized clay modifiers and to develop polymerization schemes for each polymer−clay system; however, some researchers have had great success in producing dispersions using this method. For instance, exfoliated polystyrene nanocomposites resulting from polymer chain (6−9 wt %) tethering to the clay modifier have been obtained using nitroxide-mediated in-situ polymerization.[22]

Solution mixing, although simple in its approach, has proven to be relatively ineffective at producing significant clay dispersion.[12,25−27] Appreciable exfoliation is not seen in these systems due to the thermodynamic barriers to platelet separation and potential for platelet reorganization upon solvent removal.[28] Additionally, intercalation may not occur even if there is good polymer−clay interaction because of competing effects between the polymer and the solvent for the clay modifier.[28,29] However, Zhao et al. demonstrated that if enough energy is introduced into a composite solution of polystyrene and clay in toluene, through sonication in this case, exfoliation can be achieved.[2]

Recently $scCO_2$ has been gaining popularity in research and industry as an environmentally friendly solvent and blowing agent in a wide range of applications.[30] A novel process utilizing $scCO_2$ has been developed for exfoliating layered silicate and/or graphite with or without polymer present.[31−34] The liquid-like density and gas-like diffusivity of $scCO_2$ allows it to penetrate the platelet galleries during a soaking period, while the large density change that the supercritical fluid undergoes during instantaneous depressurization pushes the platelets apart. Recently, this method has been shown to disperse natural montmorillonite in a polydimethylsiloxane matrix with the resultant nanocomposites exhibiting significant rheological improvements over the neat polymer and melt mixed benchmark.[35] It was also shown that certain clays (modifier dependent) can be exfoliated without any polymer present by soaking in $scCO_2$ followed by catastrophic depressurization. The exfoliated clay could conceivably be coextruded with the polymer of interest or it can be processed again with the polymer in the presence of $scCO_2$. In this paper, we utilize a cosolvent (styrene) to improve the processability of high molecular weight, poly-

* To whom correspondence should be addressed. Tel: 313-577-3879. Fax: 313-577-3810. E-mail: rkannan@che.eng.wayne.edu.

10.1021/ma801339g CCC: $40.75
Published on Web 10/09/2008

disperse, polystyrene in $scCO_2$ by allowing us to minimize the processing temperature. Reduction in temperature minimizes clay modifier degradation, improves CO_2 polymer miscibility, allows longer CO_2 soak times, and promotes clay−polymer contact. The choice of polydisperse polystyrene was to demonstrate the processes utility on commercial-grade polymers. The polydispersity could play a role in the chain mobility between plates and $scCO_2$ solubility. The $scCO_2$ swells the polymer rather than dissolve it. This, in conjunction with the presence of cosolvent and the long soaking times, would suggest the polydispersity does not affect the process.

The goal of the present study is to investigate the role of $scCO_2$ processing in PS/clay nanocomposites in (i) promoting polymer−clay interaction, (ii) dispersing nanoclay, and (iii) enhancing polymer thermal degradation. Improvements in nanocomposite properties are evaluated against solution-blended composites prepared using the traditional method. To gain insights into how processing parameters affect clay dispersion, polymer−clay interaction, and thermal degradation, a series of samples has been created and characterized using rheology, TEM, WAXD, and TGA. We compare the properties of the $scCO_2$-processed nanocomposites with those made through other techniques used in the literature.

2. Materials and Experimental Methods

2.1. Materials. Cloisite 10A is a natural montmorillonite clay modified with dimethyl, benzyl hydrogenated tallow (∼65 wt % C18; ∼30 wt % C16; ∼5 wt % C14) having a d_{001} spacing of 1.92 nm and was obtained from Southern Clay Products. The polystyrene used has a molecular weight of 280 000 g/mol and polydispersity of 4 and was purchased from Scientific Polymer Products, Inc. The styrene (inhibited) used in this study was purchased from Sigma Aldrich.

2.2. Wide-Angle X-ray Diffraction (WAXD). A Rigaku Rotaflex Powder Diffractometer with a Cu Kα X-ray source ($\lambda = 1.54$ Å) and an accelerating voltage of 40 kV at a current of 120 mA was used to determine the intergallery spacing of the "as-received" clays and clay/polymer nanocomposites. Samples were placed in a custom-made, zero-background quartz sample holder that is 0.9 mm in depth. Several scans were obtained from different locations in the sample and verified to be reproducible when diffraction patterns were superimposed on one another. The 2Θ angle was determined using the JADE software that accompanies the diffractometer, and the d_{001} spacing for the clays was calculated using Braggs' Law of diffraction. The intergallery spacing was then found by subtracting 1 nm (platelet thickness) from the d_{001} spacing.

2.3. Scanning Electron Microscopy (SEM). Images were collected using a Hitachi S-2400 scanning electron microscope with an electron potential of 25 kV. The samples were sputter coated with gold, and several (10−20) images per sample were collected for all samples to ensure accurate representation of the clay morphology.

2.4. Transmission Electron Microscopy (TEM). Thin films (∼80−100 nm) of the nanocomposites were prepared using a Reichert-Jung Ultracut E Microtome and placed on 200 mesh copper grids. The samples were coated with carbon prior to being examined with a JEOL Fast EM 2010 HR TEM operated at 200 kV. Numerous (10−20) images were collected for all samples to ensure accurate representation of the clay structure in the polymer matrix.

2.5. Thermogravimetric Analysis (TGA). Perkin-Elmer Pyris 1 TGA was used to measure the thermal stability of the $scCO_2$-processed nanocomposites, determine residual solvent content in the samples, verify the clay content in the composites, and determine clay modifier stability. Temperature ramp measurements were conducted under an inert atmosphere of N_2 from 25 to 650 °C at 10 °C/min.

2.6. Rheology. A Rheometric Scientific RSA II rheometer (shear sandwich geometry 15.98 mm × 12.7 mm × 0.55 mm) was used to perform melt rheological measurements under oscillatory shear.

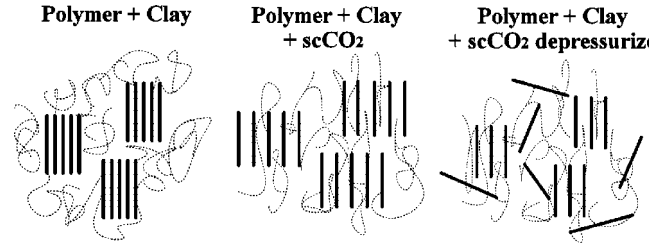

Figure 1. Illustration of the supercritical carbon dioxide process. Polymer and clay are mixed together followed by a soaking period in $scCO_2$. The system is depressurized, and the expanding CO_2 delaminates platelets.

Table 1. Nanocomposite Sample Compositions, Processing, and Nomenclature

sample name	clay wt %	processing variables
PS280	0%	none
PS-A5n	5%	solvent
PS-A5sd	5%	solvent + CO_2 (∼0.04 MPa/min)
PS-A5	5%	solvent + CO_2 + fast depress (∼300 MPa/min)
PS-A5pe	5%	solvent + CO_2 + fast depress + predispersed clay
PS-A10n	10%	solvent
PS-A10	10%	solvent + CO_2 + fast depress
PS-A2n	2%	solvent
PS-A2	2%	solvent + CO_2 + fast depress

The measurements were made under ambient air between 140 and 240 °C in 20 °C increments for all samples. Rheology measured before and after annealing at 240 °C for 2 h showed no discernible change; however, a small amount of discoloration at the edges of the samples was observed. Samples were prepared by melt pressing finely crushed nanocomposite powder into a mold at 180 °C between Teflon plates. The materials were loaded and allowed to equilibrate for 1 h at the desired temperature. Strain sweeps were performed to ensure that the dynamic moduli were independent of the strains utilized, and the linear viscoelastic measurements were made at low strains ($\gamma_o < 0.05$) to minimize microstructure destruction. The frequency range used was $0.01 \leq \omega \geq 100$ rad/s, and the property of time−temperature superposition was used to create master curves with a reference temperature of 140 °C.

2.7. Nanocomposite Formation. Polystyrene/styrene/nanoclay at a ratio of 40 g/77 g/*X* g, where *X* is the mass of clay required for each desired final weight fraction (based on polystyrene), were loaded in the reactor and mixed until homogeneous. The mixture was then processed in $scCO_2$ for 24 h at 80 °C and 13.79 MPa under constant stirring to form the nanocomposite in a 246 mL Thar Vessel equipped with a variable-speed impeller. The vessel was then rapidly depressurized to ambient pressure. The system was in solution throughout processing; therefore, no lasting foam structure was observed during the depressurization step. The above process is illustrated in Figure 1. Three samples (2, 5, and 10 wt % clay) were made using "as-received" Cloisite 10A with the above $scCO_2$ process (PS-A2, PS-A5, and PS-A10). A 5 wt % sample was also prepared which was slowly depressurized (0.046 MPa/min) (PS-A5sd) to investigate the role of $scCO_2$ soaking and depressurization rate on the resulting nanocomposite properties. Another sample was made using clay that was preprocessed in $scCO_2$ (PS-A5pe), which allows us to investigate the role of clay dispersion on the resulting polymer/clay nanocomposite properties. To eliminate the role of thermal annealing and solution blending, benchmark composites of 2, 5, and 10 wt % by clay (PS-A2n, PS-A5n, and PS-A10n) were made in the same vessel without the presence of $scCO_2$ at 80 °C for 24 h.[36] After processing, all samples were dried at room temperature for 48 h under vacuum followed by 160 °C under vacuum for 6 h to remove residual solvent. A description of the variable conditions and nanocomposite nomenclature is given in Table 1. TGA was used to validate that no residual styrene remained in the nanocomposites after drying, and gel permeation chromatography (GPC) was performed to confirm that no change in the molecular weight distribution of the polymer occurred during $scCO_2$ processing and subsequent drying of the

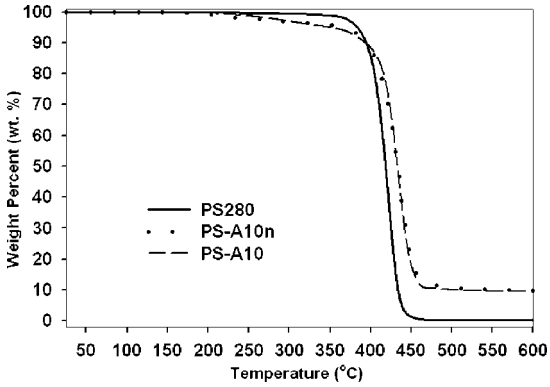

Figure 2. TGA weight-loss curves of $scCO_2$-processed 10 wt % clay nanocomposites. Thermal stability is improved upon addition of clay.

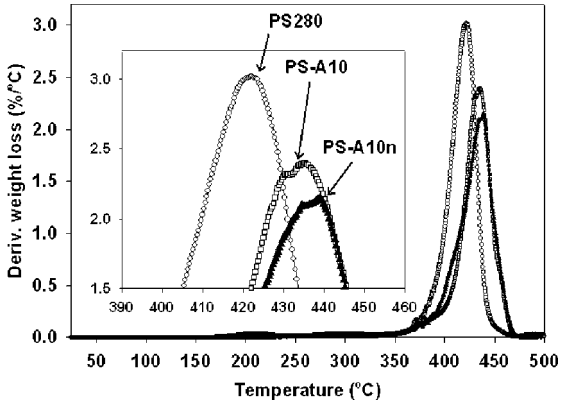

Figure 3. TGA derivative curves detailing the improvement in the maximum rate of decomposition of polymer due to nanoclay addition.

nanocomposites. TGA was performed on Cloisite 10A before and after drying to determine if clay degradation occurs during solvent removal. Notably, after 6 h at 160 °C in a vacuum, the clay shows very little loss of organic content (less than 1%) which should not significantly affect the final nanocomposite properties. WAXD was also performed on clay samples before and after annealing, and no discernible shift in d_{001} spacing was found (data not shown for brevity).

3. Results and Discussion

3.1. Thermogravimetric Analysis of Nanocomposites. TGA was performed on the $scCO_2$-processed and solution-blended 10 wt % nanocomposites (PS-A10 and PS-A10n) as well as the "as-received" polymer (PS-280) to determine any change in the thermal decomposition due to $scCO_2$ processing. Decomposition effects have been observed in many publications on nanocomposites and have mostly been attributed to polymer confinement between clay platelets.[37−41] Weight-loss curves of 10 wt % $scCO_2$-processed and solution-blended samples display a shift in decomposition to higher temperatures than the pure polymer (Figure 2). Despite the difference in processing method between the nanocomposites, the temperature at 50% weight loss is the same for both of the samples, indicating that $scCO_2$ processing has very little effect on thermal decomposition. Additionally, the lack of change in residual mass at points below 400 °C suggests that the $scCO_2$-processed composite has not lost its clay modifier during processing. TGA derivative curves are useful for determining the temperature at which the maximum rate of decomposition (MRD) occurs and more sensitive to small changes in dispersion state (Figure 3). In our system, the TGA derivative shows an increase in MRD from

Table 2. TGA Summary: Temperature at 10 and 50 wt % Weight Loss, Maximum Rate of Decompositions, and Percent Char (residual mass fraction at 600 °C)

sample name	T_{10} (°C)	T_{50} (°C)	MRD (°C)	char (%)
PS280	395.2	418.4	422.4	0.4
PS-A10	395.1	433.2	435.4	9.85
PS-A10n	394.6	433.0	439.1	9.62

422 °C for pure polystyrene to 433 and 438 °C for PS- A10 and PS-A10n, respectively (Table 2). The slightly lower MRD temperature for PS-A10 compared to PS- A10n can be attributed to a higher level of platelet dispersion and therefore a reduced amount of polymer intercalated between platelets. This result is in good agreement with previous results that show that reducing the amount of polymer intercalated between platelets also reduces the amount of relative decomposition improvement.[37] On the basis of this data, $scCO_2$ has no influence on the degradation mechanisms in polymer nanocomposites.

3.2. WAXD and SEM of Cloisite 10A. Pure Cloisite 10A was processed at 80 °C and 20.68 MPa in $scCO_2$ for 24 h followed by catastrophic depressurization in an attempt to exfoliate the clay structure without a polymer matrix present. To determine if the spacing of the clay platelets was disturbed upon processing, we probed both "as-received" and $scCO_2$-processed 10A using WAXD. The "as-received" Cloisite 10A has a diffraction peak at $2\theta = 4.7°$ corresponding to its equilibrium platelet spacing of 0.877 nm (basal spacing minus 1 nm for platelet thickness), while the $scCO_2$-processed clay shows no peak in the WAXD spectrum (Figure 4). The absence of a peak in the processed clay indicates that there is a significant reduction in parallel registry and a range of morphologies from disordered intercalated to exfoliated could be present. Similar results have been published for Cloisite 93A using the same $scCO_2$ process.[35]

To better visualize the effects $scCO_2$ has had on the structure of the clay particles and tactoids, we employed SEM to directly image the clay particles before and after $scCO_2$ processing. An SEM image along with a conceptualized cross section of a typical "as-received" 10A particle is displayed in Figure 5. The unprocessed clay is composed of particles with lateral dimensions of ∼3−20 μm consisting of a large number of tightly bound tactoids. These tactoids contain a number of highly ordered stacked platelets held together by van der Waals forces. Upon examination of a large number of SEM images, it is concluded that the tactoids are closely bound in particles and very few dispersed platelets are observed in the "as-received" samples.

In contrast, the images of $scCO_2$-processed 10A display a much different morphology (Figure 6). While a large fraction

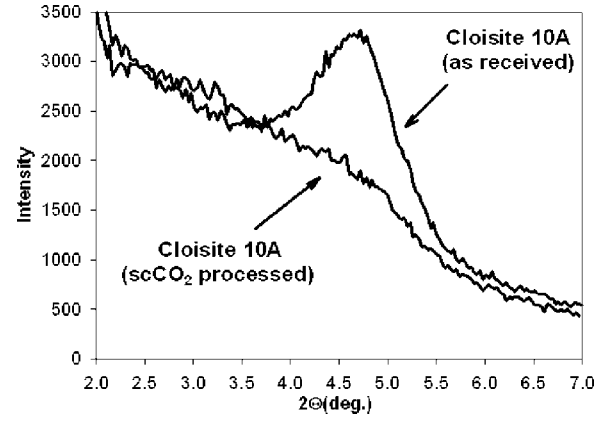

Figure 4. WAXD of "as-received" and $scCO_2$-processed Cloisite 10A. Parallel registry of the clay tactoids is lost upon depressurization, resulting in a disappearance of the X-ray diffraction peak.

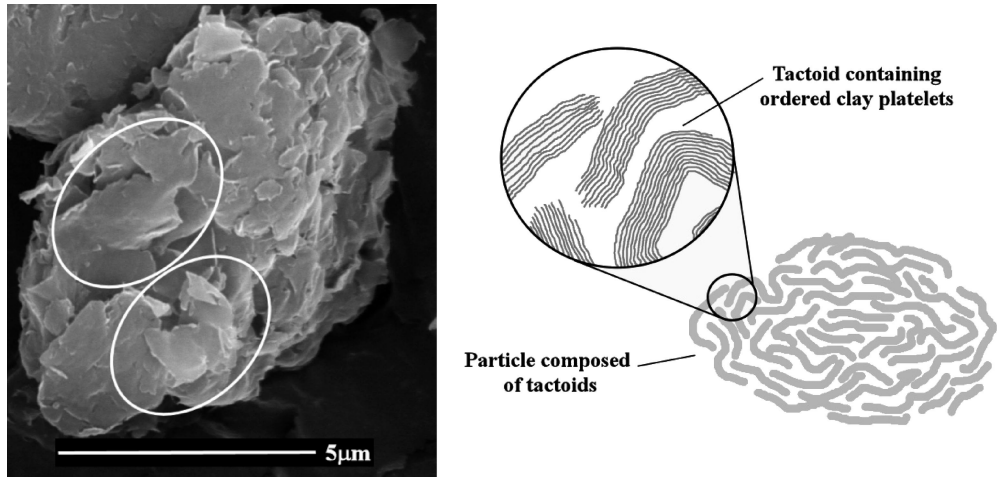

Figure 5. SEM image and illustration of "as-received" Cloisite 10A particle. Circles indicate individual tactoids/platelets.

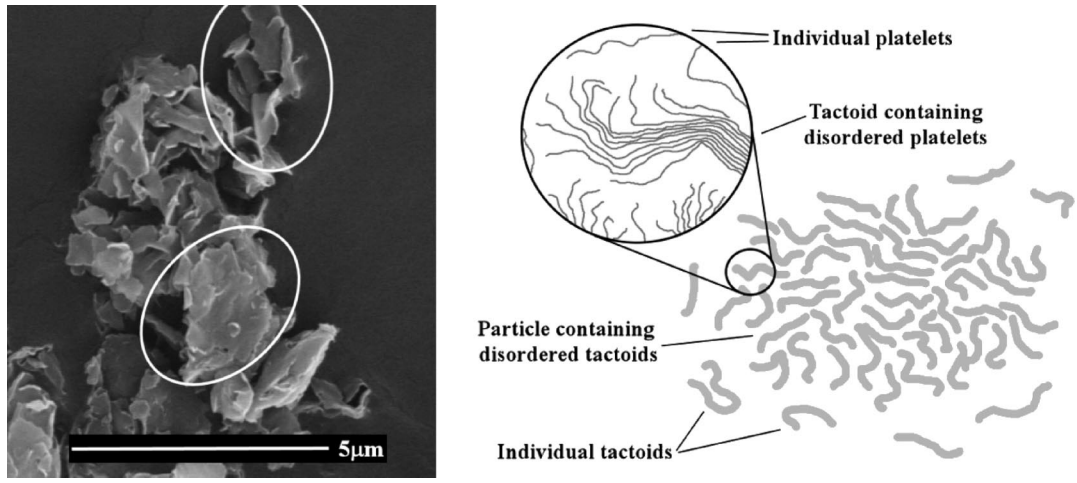

Figure 6. SEM image and illustration of $scCO_2$-processed Cloisite 10A particle. Circles indicate individual tactoids/platelets.

of tactoids is still found in particle form, the number of tactoids per particle and the tightness of packing are reduced. The individual tactoids have delaminated from each other and lost their parallel registry, leaving large spaces into the center of the aggregates for polymer to penetrate. Measuring the size of tactoids across multiple images of each material (a few of which are indicated by white circles in the figures) we find that although the average particle size has been reduced significantly, the tactoid diameter has been preserved. Upon depressurization, it appears that a fraction of the outermost layers is delaminated from the tactoids during CO_2 expansion while the much less mobile inner layers just lose the coherent parallel registry that is probed by X-ray diffraction. We qualify this system as being disordered intercalated and speculate that a relatively large fraction of the separated sheets seen in SEM may in fact be composed of a few individual platelets. Utilizing the SEM images alone we cannot confirm the existence of dispersed single layers due to the difficulty in differentiating individual platelets from individual tactoids in SEM images. In sections 3.2 and 3.4.2 we will discuss further evidence to support this description. The expanded flexible structure of the $scCO_2$-processed particles/tactoids exposes more of the available surface area, and the platelets should be easier to disperse into a polymer matrix than the "as-received" clay. This clay could possibly produce good dispersion in extrusion compounding since the kinetic limitation of clay dispersion may no longer be an issue in the short times required for melt compounding. In our study, we will add this preprocessed clay to polystyrene−styrene solution and reprocess the composite with $scCO_2$ in an attempt to maximize dispersion.

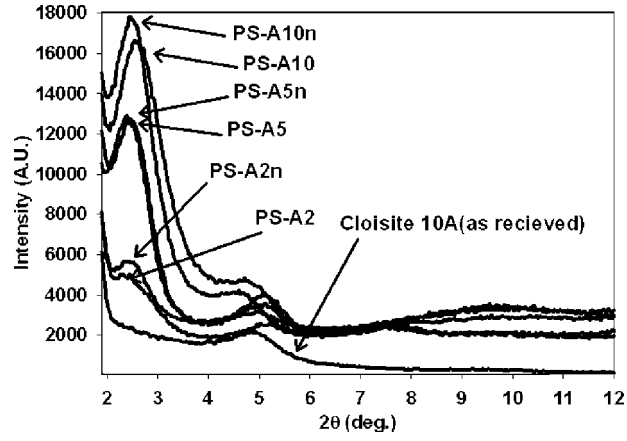

Figure 7. WAXD nanocomposites with varying weight fractions of 10A.

3.3. WAXD and TEM of PS/Clay Nanocomposites. WAXD patterns of all of the nanocomposites in this study are shown in Figures 7 and 8. All the nanocomposites exhibit a large diffraction peak at $2\theta = 2.4°$ regardless of weight fraction, processing conditions, or rheological enhancement. The shift of the peak from 4.6° for pristine 10A to 2.4° in the case of the nanocomposites corresponds to a tripling of intergallery spacing from 0.877 to 2.677 nm, suggesting that polymer has been intercalated into the clay galleries. The presence of a d_{002} peak and a tall narrow d_{001} peak indicates that the nanocomposites

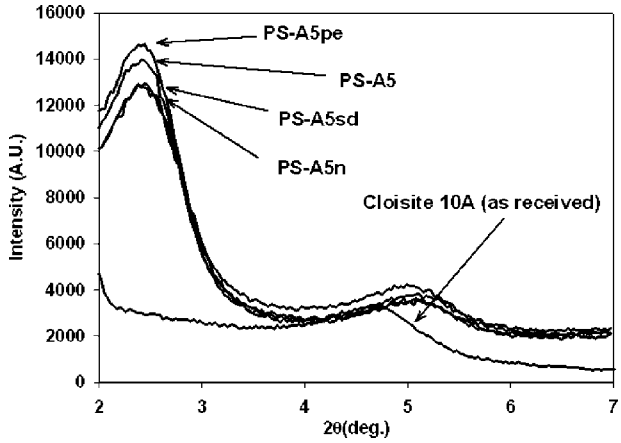

Figure 8. WAXD of 5 wt % clay nanocomposites. Peak height and location of the nanocomposites is preserved despite changes in processing conditions.

still have *some* highly ordered intercalated clay structures. Moreover, when Cloisite 10A is predispersed and recovered from solvent without polymer present, the clay recovers its equilibrium spacing of 0.877 nm (data not shown). Therefore, polymer intercalation into the clay galleries must be the cause for the clay spacing increase in the nanocomposites. Giannalis and Vaia previously modeled the intercalation behavior of clay in the presence of polymer and determined that there are a number of factors that contribute to the level of intercalation/exfoliation that is attainable in a given system. The findings were substantiated by performing corresponding experiments on several PS/clay systems.[28,42] They found that there is an entropic balance between the clay modifier wanting to have as much conformational freedom as possible and the matrix polymer not wanting to be confined between the platelets. There is a continuous entropic gain experienced by the organic modifier until the basal spacing is increased to the point where the surfactant chains can be fully extended (h_∞); additional expansion does not result in more entropy. However, even when the clay galleries are expanded to maximize the surfactant entropy the separation is still small enough that typical polymers will have restricted motion when occupying the space between platelets. In order for the platelets to extend farther than h_∞, very strong interactions between the polymer and the clay to overcome the entropic barrier would be required. The intergallery spacing at full chain extension (h_∞) can be expressed in terms of the number of carbon atoms in the aliphatic backbone (n') by

$$h_\infty = (n' - 1)0.127 + A + B \quad (1)$$

where A and B represent the size of a methyl and an ammonium moiety, respectively.[43]

Our system is processed in a good solvent for the clay modifier; the aliphatic chains on the clay surface are fully extended. This correlates to a calculated spacing of approximately 2.4 nm, which compares favorably with the experimentally measured intergallery spacing of 2.6 nm. However, since there is also polymer in solution the barrier to exfoliation of the ordered platelets is too great to overcome, leading to at least some fraction of the sample being ordered and highly intercalated.

An interesting point to note is the behavior of the predispersed clay when processed with polymer and solvent. Even though the clay itself was $scCO_2$ processed and WAXD displayed no measurable order (Figure 4), upon addition to solution it regains *some* of its parallel registry. It has been shown previously that disordered intercalated systems will not give an X-ray peak even if the platelets are still quite close together.[44] If the platelets in the clay have not been exfoliated and instead have lost their ordered spacing, it is possible that the solvent allows the dynamic reorganization of some platelets to their original spacing. The presence of polymer between the dispersed platelets may prevent reorganization of platelets that are not in close proximity, resulting in a composite with a bimodal population of small ordered tactoids and dispersed platelets/platelet pairs. WAXD is not sensitive to dispersed platelets and therefore may not be representative of the true dispersion state of the system; however, a higher level of dispersed platelets and smaller tactoids should be evident in rheology (see section 3.4.2).

Transmission electron microscopy was also utilized to characterize the state of dispersion and the morphology of clay in the nanocomposites. Images of 10 wt % $scCO_2$-processed and control composites (Figure 9a−d) were collected at low and high magnification. The images show a high level of homogeneity in both samples with no areas of unusually high or low concentrations of clay evident. Measuring the size of 50 representative tactoids from each sample over multiple images tells us that the average tactoid thickness in the $scCO_2$ material is 31 ± 23 nm, while the average in solution is approximately 158 ± 36 nm. Utilizing the d_{001} spacing found by WAXD we calculate this to be equivalent to approximately 9 platelets and 42 platelets per tactoid, respectively, with the large standard deviation in the $scCO_2$ sample coming from the presence of many single- and double-platelet tactoids. The 4-fold decrease in tactoid size upon $scCO_2$ processing results in an increase in available surface area in addition to the increase due to dispersed individual platelets. The interactions between the Cloisite 10A phenyl group and polystyrene could be favorable, and an increase in surface area can directly translate to improved material properties as will be discussed later (see section 3.4).

We can conclude that $scCO_2$ processing produces a more complex morphology with a large fraction of dispersed platelets when compared to solution blending alone. Rheology is a more sensitive tool to the degree of dispersion and polymer−clay interactions and will be used to better characterize the increase in dispersion received with $scCO_2$ processing.

3.4. Viscoelastic Behavior of PS/Clay Nanocomposites. We investigated the roles that CO_2, depressurization rate, clay weight fraction, and clay predispersion play in affecting the micro/mesoscale structure and interactions in our nanocomposites by measuring the viscoelastic response. In order to quantify the changes in dispersion and polymer−clay interaction for each of our processed composites, a 5 wt % benchmark solution-blended sample was prepared. The solution-blended PS-A5n, representing our benchmark sample, shows the onset of a low-frequency plateau in storage modulus around 10^3 dyn/cm^2 (Figure 10) similar to results in the literature on solution-blended polystyrene nanocomposites.[2,22] The morphology of this composite is suspected to be purely intercalated as supported by the previously discussed TEM images of the 10 wt % solution-blended composite (Figure 9). Furthermore, the results are in good agreement with recent work which also showed that solution blending alone in polystyrene composites produces intercalated morphologies.[22,27]

3.4.1. Effect of $scCO_2$ Depressurization Rate. The temperature and pressure were chosen to allow for significant reduction in viscosity so that mixing is possible during contacting. Our prior results suggest that the high pressure and solvation effect of $scCO_2$ during processing as well as the dramatic expansion of CO_2 during depressurization are both contributors to the overall effectiveness of the process.[35,45] The current method utilizes substantial $scCO_2$ contact time and has been previously shown to improve dispersion and interactions in other systems alone.[35,45] This differs from other processes that use $scCO_2$ as

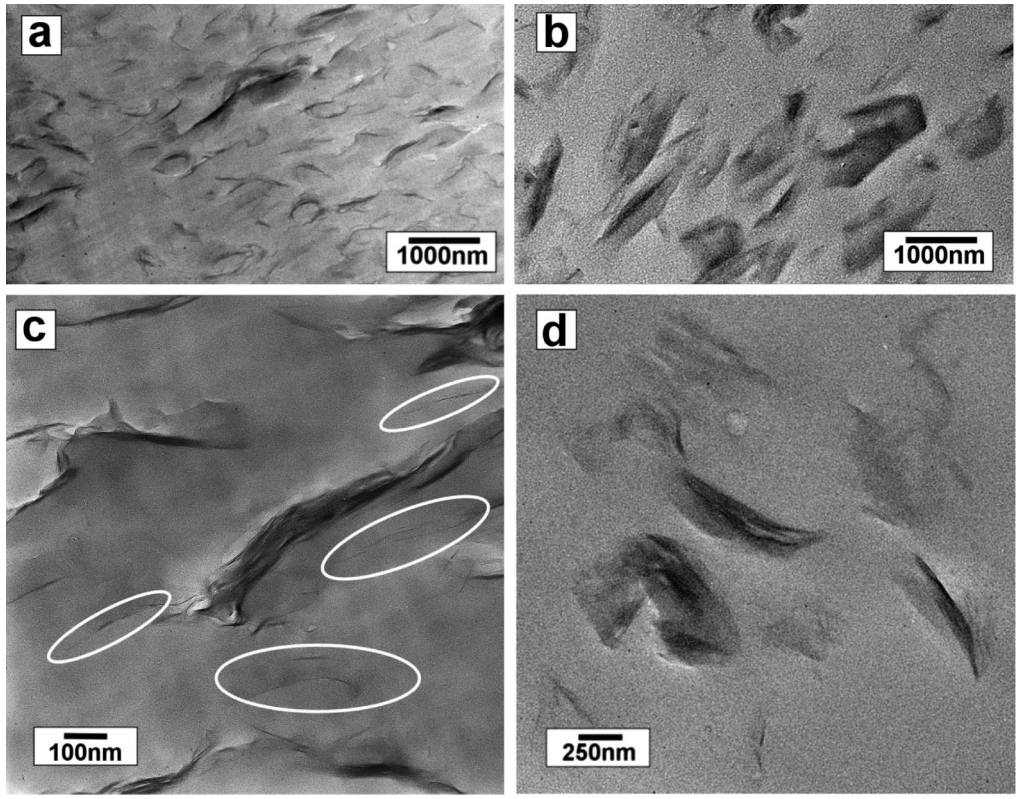

Figure 9. TEM images of 10 wt % 10A nanocomposites: (a) low-magnification $scCO_2$-processed [PS-A10], (b) low-magnification solution-blended [PS-A10n], (c) high-magnification $scCO_2$-processed [PS-A10], (d) high-magnification solution-blended [PS-A10n]. White circles indicate individual platelets. Images a and b are at the same magnification; however, image c was taken at 2.5 times higher magnification than image d in order to resolve the presence of individual platelets in the $scCO_2$ sample (image c). No individual platelets were found at higher magnification of the solution-blended sample (image d).

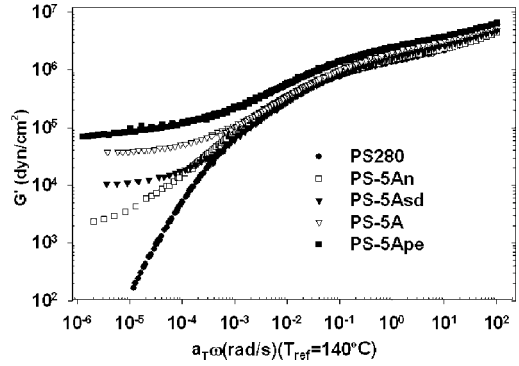

Figure 10. Storage modulus of polystyrene and 5 wt % 10A nanocomposites. Solid-like behavior at low frequencies is enhanced with improved level of dispersion.

a processing aid in extrusion with relatively little contact time and those that use high mechanical pressures.[46,47]

After the appropriate choice of temperature and pressure are made, the $scCO_2$ depressurization rate can be the next critical step in dispersing clay platelets and effectively maximizing the clay surface area available for polymer−clay interaction. To understand this, two solution-blended samples were processed in $scCO_2$ for 24 h at 13.79 MPa and 80 °C and depressurized at different rates to investigate how influential rapid CO_2 expansion is in producing clay dispersion. One sample was depressurized very slowly (approximately 0.046 MPa/min) over a 5 h period (sample PS-A5sd), while the other was depressurized very quickly (approximately 400 MPa/min) over a 2 s period (sample PS-A5). During fast depressurization, measuring the sample temperature is difficult. It is possible that during the depressurization the sample may undergo cooling. This cooling effect, we believe, is not substantial since we have a large a steel vessel and a large solution of the sample at 80 °C with only moderate amounts of CO_2.

During slow depressurization we should minimize the effect that $scCO_2$ depressurization has on the structure of the clay in the resultant sample because much of the CO_2 may have time to diffuse out of the clay galleries. PS-A5sd displays a 6-fold increase in G' at low frequencies relative to the solution-blended sample, suggesting that even at slow rates of depressurization an increase in the extent of polymer−clay interaction has occurred. The effect that $scCO_2$ had on dispersion in melt-extruded nylon-6 nanocomposites was recently investigated.[46] The authors found that the presence of $scCO_2$ during melt processing produces no significant change in the X-ray diffraction peak. The length of time that a given sample of nanocomposite is in contact with $scCO_2$ is not shown; however, it can be assumed that since it was a continuous extrusion process the contact time was relatively short. This underscores the necessity of providing sufficient time for the $scCO_2$ to diffuse into the clay galleries before depressurizing, especially when in the melt state, where the $scCO_2$ diffusion rate will be reduced when compared to solution.

To further probe the effect of depressurization rate, we compare the slow depressurized PS-A5sd against a composite that has been depressurized nearly instantaneously (PS-A5). Both PS-A5 and PS-A5sd samples were processed in $scCO_2$, which allows us to neglect the effect of $scCO_2$ on promoting polymer−clay interactions, and the resulting differences in clay dispersion between these samples should reflect the difference in depressurization rate. PS-A5 shows a 5-fold improvement in G' at low frequencies over the PS-A5sd sample, even though the slow depressurized sample already displays a dramatic improvement over the pure polymer. These support the TEM

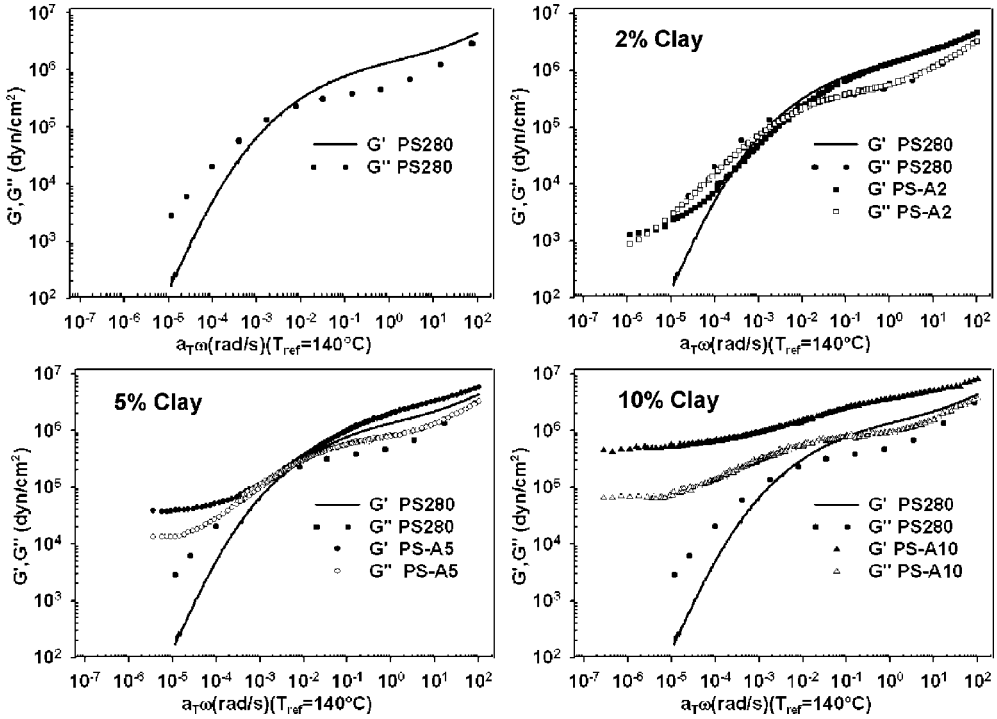

Figure 11. Oscillatory shear rheology master curves for the 280k PS and PS/10A nanocomposites created from frequency sweeps from 140 to 240 °C. Above 5% clay the storage modulus dominates the loss modulus for the entire frequency range.

images showing improved dispersion (Figure 9) and suggest that the rate at which $scCO_2$ escapes does in fact have a significant effect on the resulting nanocomposite structure. When the system is depressurized instantaneously, the $scCO_2$, which diffused in between clay layers during processing, undergoes a large change in density and effectively pushes the platelets apart. This process does not produce as much dispersion when the system is slowly depressurized since $scCO_2$ has a much longer time to diffuse out of the clay galleries. This effect of depressurization is qualitatively the same as prior results on pure clays and polymer/clay systems with no solvent.[45]

3.4.2. Effect of Clay Predispersion. It was earlier demonstrated that Cloisite 10A may be dispersed through $scCO_2$ processing without the presence of polymer. Now we reprocess the predispersed clay in the presence of polystyrene/styrene solution in an attempt to produce additional clay dispersion. This is examined by following the previous fast depressurization protocol but with predispersed 10A (sample PS-A5pe). The WAXD pattern of this sample is similar to that of PS-A5 (Figure 8); however, the storage modulus of the PS-A5pe sample once again exhibits an enhancement over the PS-A5 sample even though both samples exhibit the same d_{001} peak. When predispersed clay is reprocessed we expect that the tactoid size will be reduced further and that there will be even more surface area available for polystyrene−clay contact. This is evident in the storage modulus, which displays a 2-fold increase in G' over the already highly reinforced PS-A5 sample containing "as-received" clay. This result supports the earlier speculation that some of the individual structures observed in SEM were in fact dispersed platelets.

Rheology has been demonstrated to be an effective tool to quantify the improvements in mechanical response that result from attempting to maximize clay dispersion and/or interactions. In-situ polymerization has been shown to give the highest levels of dispersion and rheological reinforcement in polystyrene nanocomposites. In a recent work by Zhong and co-workers, clay modified with two different functionalities was used in an in-situ-polymerized polystyrene system to produce a high molecular weight (300 000 g/mol) nanocomposite.[25] The polystyrene was chemically bonded to the clay surface, resulting in an exfoliated polymer hybrid that they theorize has increased polystyrene−clay interaction and compatibility over solution-blended composites. Despite the high level of processing complexity, strong polymer adhesion to clay, and high level of dispersion in this system, the rheological enhancement measured was similar in magnitude to the current $scCO_2$-processed polystyrene nanocomposite. This suggests that $scCO_2$-induced polymer−clay interaction may be contributing significantly in our system, producing similar levels of viscoelastic reinforcement despite having a lower apparent clay exfoliation. This is further evidenced when comparing our system to an in-situ-polymerized system that is largely intercalated rather than exfoliated.[40] The authors measure 1 order of magnitude improvement in storage modulus over pristine polymer in a 5 wt % nanocomposite. Comparatively we show nearly 3 orders of magnitude improvement at similar frequencies and clay loadings. This further reinforces the conclusion that polymer−clay interactions strongly affect the resultant properties of polystyrene nanocomposites and $scCO_2$ processing promotes such interactions.

3.4.3. Effect of Clay Weight Fraction. Finally, the effect of nanoclay weight fraction on the viscoelastic properties of the nanocomposites was studied. As described earlier, both the $scCO_2$-processed and the benchmark composites show the same intercalation peak in XRD regardless of clay content. At weight fractions as low as 2 wt % clay, the PS-A2 sample exhibits the emergence of a low-frequency plateau in G', effectively creating a second crossover frequency. However, the original crossover remains unchanged, suggesting that at 2 wt % clay the matrix relaxation time may not be substantially altered (Figure 11). The benchmark analog sample (PS-A2n) which shows no improvement in G' compared to pristine polystyrene (Figure 12). The appearance of a plateau at low frequencies indicates a change in relaxation dynamics of the platelets due to formation of a percolated particle network. A relationship between the number of platelets per tactoid and the percolation threshold has been suggested by Ren et al.[12]

$$\eta_{per} = \frac{4}{3\varphi_{per}}\left[\frac{w_{sil,per}\rho_{org}}{w_{sil,per}\rho_{org} + (1 - w_{sil,per})\rho_{sil}}\right]\frac{R_h}{h_{sil}}$$

where η_{per} is the average number of platelets per tactoid, $\Phi_{per} \approx 0.3$ (percolation for spherical domain), $w_{sil,per}$ is the weight fraction of silicate at the percolation threshold, R_h is the average radius of a platelet, ρ_{org} is the density of the host polymer, ρ_{sil} is the density of the silicate, and h_{sil} is the thickness of a platelet. The average platelet radius calculated from SEM images is 500 nm, and the average number of platelets per tactoid was estimated from TEM to be 31 and 9 for the solution-blended and $scCO_2$ samples, respectively. Using the above equation the percolation threshold in the $scCO_2$ composite was calculated be 0.7% and for the solution-blended composite 2.5%. The result correlates well with our rheology data that indicates percolation in PS-A2 but not in PS-A2n, further supporting that $scCO_2$ processing can provide significant dispersion and reinforcement even at relatively low weight fractions. Accordingly, when we increase the weight fraction of clay to 5%, the solution-blended composite should also exhibit a low-frequency plateau. When we examine the terminal range of the 5% composites, the solution-blended composite shows the emergence of a plateau while G' is enhanced and both of the crossover frequencies have vanished in $scCO_2$-processed PS-A5. This sample shows a 40% increase in G′ at high frequencies and more than two-order of magnitude reinforcement at low frequencies over pure polymer. Furthermore, the storage modulus of the 5 wt % $scCO_2$ sample becomes larger than even the 10 wt % solution-blended sample (PS-A10n) at shifted frequencies below 3×10^{-5} rad/s despite having one-half of the clay content. At 10 wt % clay we have reached a point of total domination of G' over G″ for PS-A10 with both becoming nearly frequency independent for the entire range probed. We observed that the 10 wt % composite processed in $scCO_2$ shows more than an order of magnitude increase in the low-frequency plateau range over the benchmark counterpart and more than 3 orders of magnitude compared to PS.

Recent work in solution blending shows similar results to our benchmark composites at various clay loadings.[26,27] Sohn and co-workers saw no improvement at low clay loadings; however, they obtain an order of magnitude increase in an intercalated 10 wt % nanocomposite. Although we also showed no improvement at low clay loadings for solution-blended composites, our $scCO_2$-processed 2% composite displayed an improvement comparable to their 10 wt % sample at low frequencies. This clay weight fraction study further substantiates the conclusion that $scCO_2$ processing of polymer nanocomposites leads to improved clay dispersion and interactions.

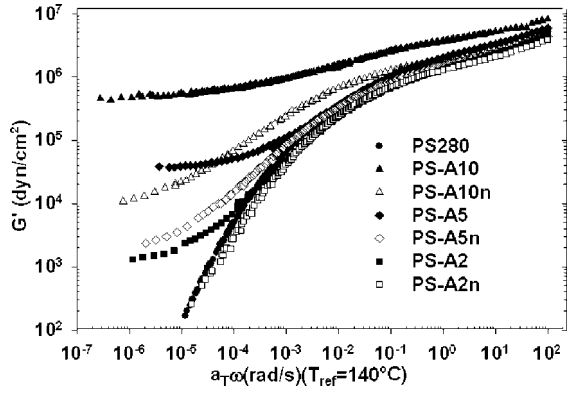

Figure 12. Storage modulus of polystyrene and nanocomposites with varying weight fractions of 10A. Percolation is observed in $scCO_2$-processed samples (2 wt %) at lower weight fractions than in solution-blended samples (5 wt %).

4. Conclusions

A novel technique utilizing soaking in supercritical CO_2 followed by fast depressurization was used to disperse 'as-received' Cloisite 10A and create a series of high molecular weight polystyrene−clay nanocomposites with significant dispersion and rheological enhancement. The effects of depressurization, filler concentration, and nanoclay predispersion on nanocomposites produced in solution were investigated by WAXD, TEM, SEM, TGA, and rheology.

Cloisite 10A was successfully disordered upon depressurization of $scCO_2$ without the presence of an organic phase as determined by the absence of a d_{001} diffraction peak in WAXD data. Furthermore, SEM images revealed a disruption of the tactoids from a tightly bound morphology to a disordered loosely associated structure with a fraction of individual platelets present. Upon addition to polystyrene−styrene solution it was found that some portion of the clay regains its parallel registry, as evident by the reappearance of a defined X-ray diffraction peak. Even though the final product has the same WAXD peak as a solution-blended sample, a nanocomposite using predispersed clay shows significant rheological improvement, indicating a higher level of dispersion. This suggests that the large particles are predominately responsible for the diffraction peaks and that disorder of the platelets on the surface of these particles significantly reduces the diffraction signature. Once in a solvent, the favorable energy reduction realized by reducing platelet distortion can overcome the entropic penalty of reordering.

Processing clay/polymer solution in $scCO_2$ followed by quick depressurization leads to further reinforcement of the matrix compared to slowly depressurizing, implying that the dramatic CO_2 expansion is a key factor in producing dispersion with this process. Our results show that this processing method not only allows improved clay dispersion but also promotes polymer−clay interaction. At 5 wt% clay loading, the $scCO_2$ processed nanocomposites show a 40-fold enhancement in the low frequency "plateau" elastic modulus compared to solution blended benchmark. The results from this process appear to be comparable to or better than processes that use 'custom-modified' clays with in-situ polymerization.[25]

Acknowledgment. Funding from the NSF CTS 0335315 (Kannan, nanoSEC NSF SBIR Phase II subcontract) and WSU-Institute of Manufacturing Research are greatly appreciated. We would like to thank Dr. Liu for assistance in acquiring TEM images.

References and Notes

(1) Gorrasi, G.; Tortora, M.; Vittoria, V.; Pollet, E.; Lepoittevin, B.; Alexandre, M.; Dubois, P. *Polymer* **2003**, *44* (8), 2271–2279.
(2) Zhao, J.; Morgan, A. B.; Harris, J. D. *Polymer* **2005**, *46*, 8641–8660.
(3) Gopakumar, T. G.; Lee, J. A.; Kontopoulou, M.; Parent, J. S. *Polymer* **2002**, *43* (20), 5483–5491.
(4) Blumstein, A. *J. Polym. Sci., A: Gen. Pap.* **1965**, *3* (7), 2653–64.
(5) Kuznetsov, D. V.; Balazs, A. C. *J. Chem. Phys.* **2000**, *112* (9), 4365.
(6) Yu, M.; Zhang, Q.; Fu, Q. *Chin. J. Polym. Sci.* **2003**, *22* (1), 43–47.
(7) Chow, W. S.; Ishak, Z. A. *Polym. Lett.* **2007**, *1* (2), 77–83.
(8) Ma, J.; Yu, Z.-Z.; Zhang, Q.-X.; Xie, X.-L.; Mai, Y.-W.; Luck, I. *Chem. Mater.* **2004**, *16* (5), 757–759.
(9) Maarouf, B. T.; Bagher, R. *Iranian J. Polym. Sci. Technol. (Persian Ed.)* **2007**, *20* (1), 59–64.
(10) Galgali, G.; Ramesh, C.; Lele, A. *Macromolecules* **2001**, *34* (3), 852–858.
(11) Wang, H.; Zeng, C.; Elkovitch, M.; Lee, L. J.; Koelling, K. W. *Polym. Eng. Sci.* **2004**, *41* (11), 2036–2046.
(12) Ren, J.; Silva, A. S.; Krishnamoorti, R. *Macromolecules* **2000**, *33*, 3739–3746.
(13) Solomon, M. J.; Almusallam, A. S.; Seefeldt, K. F.; Somwangthanaroj, A.; Varadan, P. *Macromolecules* **2001**, *34*, 1864–1872.
(14) Lim, Y. T.; Park, O. O. *Macromol. Rapid Commun.* **2000**, *21* (5), 231–235.
(15) Lim, Y. T.; Park, O. O. *Rheol. Acta* **2001**, *40* (3), 1435–1528.

(16) Meincke, O.; Hoffmann, B.; Dietrich, C.; Friedrich, C. *Macromol. Chem. Phys.* **2003**, *204* (5−6), 823–830.
(17) Tanoue, S.; Utracki, L. A.; Garcia-Rejon, A.; Sammut, P.; Ton-That, M.-T.; Pesneau, I.; Kamal, M. R.; Lyngaae-Jørgensen, J. *Polym. Eng. Sci.* **2004**, *44* (6), 1061–1076.
(18) Tanoue, S.; Utracki, L. A.; Garcia-Rejon, A.; Tatibouët, J.; Cole, K. C.; Kamal, M. R. *Polym. Eng. Sci.* **2004**, *44* (6), 1046–1060.
(19) Ray, S. S.; Okamoto, M. *Prog. Polym. Sci.* **2003**, *28* (11), 1539–1641.
(20) Li, J.; Xu, Q.; Peng, Q.; Pang, M.; He, S.; Zhu, C. *J. Appl. Polym. Sci.* **2006**, *100* (1), 671–676.
(21) Zhu, J.; Uhl, F. M.; Morgan, A. B.; Wilkie, C. A. *Chem. Mater.* **2001**, *13* (12), 4649–4654.
(22) Xu, L.; Reeder, S.; Thopasridharan, M.; Ren, J.; Shipp, D. A.; Krishnamoorti, R. *Nanotechnology* **2005**, *16* (7), S514−S521.
(23) Okamoto, M.; Morita, S.; Taguchi, H.; Kim, Y. H.; Kotaka, T.; Tateyama, H. *Polymer* **2000**, *41* (10), 3887–3890.
(24) Zhao, Q.; Samulski, E. T. *Polymer* **2006**, *47* (2), 663–671.
(25) Zhong, Y.; Zhu, Z.; Wang, S.-Q. *Polymer* **2005**, *46* (9), 3006–3013.
(26) Sohn, J. I.; Lee, C. H.; Lim, S. T.; Kim, T. H.; Choi, H. J.; Jhon, M. S. *J. Mater. Sci.* **2003**, *38* (9), 1849–1852.
(27) Han, S. S.; Kim, Y. S.; Lee, S. G.; Lee, J. H.; Zhang, K.; Choi, H. J. *Macromol. Symp.* **2006**, *245−246* (1), 199–207.
(28) Vaia, R. A.; Giannelis, E. P. *Macromolecules* **1997**, *30* (25), 7990–7999.
(29) Theng, B. K. G. *Formation and Properties of Clay-Polymer Complexes*; Elsevier: New York, 1979.
(30) Tomasko, D.; Li, H.; Liu, D.; Han, X.; Wingert, M. J.; Lee, L. J.; Koelling, K. *Ind. Eng. Chem. Res.* **2003**, *42* (25), 6431–6456.
(31) Manke, C. W.; Gulari, E.; Mielewski, D. F.; Lee, E. C.; Gulari, E.; Mielewski, D. F.; Lee, E. C. System and method of delaminating a layered silicate material by supercritical fluid treatment. Patent 6469073, Oct 2002.
(32) Mielewski, D. F.; Lee, E. C.; Manke, C. W.; Gulari, E. System and method of preparing a reinforced polymer by supercritical fluid treatment. Patent 6753360, Jun 2004.
(33) Gulari, E.; Serhatkulu, G. K.; Kannan, R. Method of delaminating aggregated particles with a coating agent in a supercritical fluid. Patent 7387749, Feb 2004.
(34) Gulari, E.; Serhatkulu, G. K. Method of delaminating a graphite structure with a coating agent in a supercritical fluid. Patent 7157517, Jul 2003.
(35) Horsch, S.; Serhatkulu, G.; Gulari, E.; Kannan, R. M. *Polymer* **2006**, *47* (21), 7485–7496.
(36) Kojima, Y.; Usuki, A.; Kawasumi, M.; Okada, A.; Kurauchi, T.; Kamigaito, O. *J. Polym. Sci., A: Polym. Chem.* **1993**, *31* (7), 1755.
(37) Morgan, A. B.; Chu, L.; Harris, J. D. *Fire Mater.* **2005**, *29*, 213–229.
(38) Doh, J. G.; Cho, I. *Polym. Bull.* **1998**, *41*, 511–518.
(39) Zhu, J.; Wilkie, C. A. *Polym. Int.* **2000**, *49*, 1158–1163.
(40) Qi, R.; Jin, X.; Nie, J.; Yu, W.; Zhou, C. *J. Appl. Polym. Sci.* **2005**, *97* (1), 201–207.
(41) Dong, Z.; Liu, Z.; Zhang, J.; Han, B.; Sun, D.; Wang, Y.; Huang, Y. *J. Appl. Polym. Sci.* **2004**, *94* (3), 1194–1197.
(42) Vaia, R. A. P.; Giannelis, E. *Macromolecules* **1997**, *30* (25), 8000–8009.
(43) Brindley, G. W.; Brown, G. *Crystal Structure of Clay Minerals and their X-ray Diffraction*; Mineralogical Society: London, 1980.
(44) Morgan, A. B.; Gilman, J. W. *J. Appl. Polym. Sci.* **2003**, *87* (8), 1329–1338.
(45) Horsch, S. *Supercritical CO_2 Dispersion of Nano-clays and Characterization of Polymer Clay Nanocomposites*. Ph.D. Thesis, Wayne State University, Detroit, MI, **2006**.
(46) Yang, K.; Ozisik, R. *Polymer* **2006**, *47* (8), 2849–2855.
(47) Saitoa, T.; Okamotoa, M.; Hiroib, R.; Yamamotob, M.; Shiroib, T. *Polymer* **2007**, *48* (14), 4143–4151.

MA801339G